

CAPE in Tropical Cyclones

JOHN MOLINARI

Department of Atmospheric and Environmental Sciences, University at Albany, State University of New York, Albany, New York

DAVID M. ROMPS

Department of Earth and Planetary Science, University of California, Berkeley, and the Earth Sciences Division, Lawrence Berkeley National Laboratory, Berkeley, California

DAVID VOLLARO AND LEON NGUYEN

Department of Atmospheric and Environmental Sciences, University at Albany, State University of New York, Albany, New York

(Manuscript received 3 October 2011, in final form 13 February 2012)

ABSTRACT

Convective available potential energy (CAPE) and the vertical distribution of buoyancy were calculated for more than 2000 dropsonde soundings collected by the NOAA Gulfstream-IV aircraft. Calculations were done with and without the effects of condensate loading, entrainment, and the latent heat of fusion. CAPE showed larger values downshear than upshear within 400 km of the center, consistent with the observed variation of convective intensity. The larger downshear CAPE arose from (i) higher surface specific humidity, (ii) lower midtropospheric temperature, and, for entraining CAPE, (iii) larger free-tropospheric relative humidity.

Reversible CAPE had only one-half the magnitude of pseudoadiabatic CAPE. As shown previously, reversible CAPE with fusion closely resembled pseudoadiabatic CAPE without fusion. Entrainment had the most dramatic impact. Entraining CAPE was consistent with the observed radial distribution of convective intensity, displaying the largest values downshear at inner radii. Without entrainment, downshear CAPE was smallest in the core and increased outward to the 600-km radius.

The large number of sondes allowed the examination of soundings at the 90th percentile of conditional instability, which reflect the conditions leading to the most vigorous updrafts. Observations of convection in tropical cyclones prescribe the correct method for calculating this conditional instability. In particular, the abundance and distribution of vigorous deep convection is most accurately reflected by calculating CAPE with condensate retention and a fractional entrainment rate in the range of 5%–10% km⁻¹.

1. Introduction

The azimuthal asymmetry of convection in tropical cyclones experiencing vertical wind shear has been described extensively. Corbosiero and Molinari (2002, 2003) examined the cloud-to-ground lightning distribution in tropical cyclones. The ratio of downshear to upshear flashes was 6:1 overall, and more than 9:1 when ambient vertical wind shear exceeded 5 m s⁻¹. Inside the 100-km radius, the lightning frequency maximum

occurred in the downshear-left quadrant, while from 100 to 300 km the maximum shifted to downshear right. Abarca et al. (2011) updated these results using a long-range network that sampled storms over open ocean as well as near land. The vast majority of electrified convection outside the 100-km radius occurred downshear or downshear right.

Molinari and Vollaro (2010) showed that convective available potential energy (CAPE) averaged from 75- to 400-km radii was 60% larger downshear than upshear. They hypothesized that the larger CAPE arose from stronger upward motion downshear producing negative midlevel temperature anomalies. Nguyen et al. (2010) showed that such anomalies existed. The presence of larger CAPE might account for the more frequent

Corresponding author address: John Molinari, Department of Atmospheric and Environmental Sciences, ES-225, University at Albany/SUNY, 1400 Washington Avenue, Albany, NY 12222.
E-mail: jmolinari@albany.edu

downshear convection, but Molinari and Vollaro (2010) examined only 100 sondes and calculated only pseudoadiabatic CAPE.

For many years a debate has existed in the literature regarding the most meaningful way to calculate CAPE and how to interpret the result. Two examples are pseudoadiabatic CAPE, for which all condensate is assumed to immediately fall from the parcel, and reversible CAPE, for which all condensed water remains with the parcel. Reversible CAPE without the latent heat of fusion is much smaller than pseudoadiabatic CAPE owing to the weight of condensates. Xu and Emanuel (1989) noted that the tropics are nearly neutral to reversible ascent from the top of the mixed layer when condensate loading is included and fusion is excluded.

Romps and Kuang (2010), using cloud-resolving simulations of tropical deep convection, found that the fraction of undilute parcels fell below 1% above a height of 4 km. This suggests that some form of entrainment must be incorporated into parcel buoyancy estimates. Wei et al. (1998) found that entrainment had 4 times the impact of condensate loading in reducing CAPE. Holloway and Neelin (2009) showed that entrainment was required to account for the observed correlation between column-integrated water vapor and precipitation in the tropics. The reduction of buoyancy due to entrainment of relatively dry air played a major role in inhibiting precipitation in their model. DeMaria (2009) developed a logistic regression model for tropical cyclone intensity prediction. One key input variable was a simulated parcel vertical velocity based on the buoyancy of the parcel within the mean tropical cyclone environment. DeMaria (2009) showed that both entrainment and water loading were needed to produce realistic results. Overall, the results from these papers suggest that the effects of entrainment should be represented in order for CAPE to be meaningful.

Many studies have also noted the importance in CAPE calculations of heating arising from the freezing of condensate. Williams and Renno (1993) and Emanuel (1994; see his Fig. 14.4) showed that the increase in CAPE from fusion heating offset the decrease in CAPE from condensate loading. As a result, reversible CAPE with fusion differed little from the pseudoadiabatic value without fusion.

Zipser (2003), Romps and Kuang (2010), and Fierro et al. (2012) provided considerable evidence, both from observations and cloud-resolving models, that convective clouds in the tropics can reach the tropopause only as a result of the release of the latent heat of fusion. Clouds in tropical cyclones often reach to and sometimes beyond the tropopause (e.g., Romps and Kuang 2009). Consistent with this, Heymsfield et al. (2010)

found maximum vertical velocity in tropical cyclone convection near the 12-km level. The evidence from these papers argues for the importance of fusion heating.

With the exception of the work by DeMaria (2009), neither entrainment nor fusion has been included in the calculation of CAPE in tropical cyclone studies. The tropical cyclone provides a useful laboratory for investigating CAPE because deep convection develops much more frequently at small radii than large (e.g., Frank 1977) and lightning occurs much more frequently downshear than upshear (Corbosiero and Molinari 2002). In this paper, the primary focus will be on the radial and azimuthal distributions of CAPE and convective inhibition (CIN) and the vertical distribution of buoyancy. These will be calculated following Romps and Kuang (2010) from more than 2000 dropsondes released from high altitudes. The relationship between buoyancy, CAPE, CIN, and tropical cyclone convection will be addressed, as well as the optimum calculation of CAPE.

2. Data sources and calculation methods

a. Data

All data for this study come from GPS sondes (Hock and Franklin 1999) that were released in tropical cyclones by the National Oceanic and Atmospheric Administration (NOAA) Gulfstream-IV (G-IV) aircraft. Sondes were restricted to within 1000 km of the center of tropical cyclones and with release levels above 400 hPa. The sondes were processed using Editsonde software by the Hurricane Research Division of NOAA. The data cover 32 storms over 7 yr (1997–99; 2002–05). Only 3% of these sondes were released in tropical depressions, and 24% in tropical storms; the remainder were released in hurricanes across all intensity ranges.

Any data marked as questionable by Editsonde were removed. These included data from the first 30 s (~600 m) of the sounding during which the sonde adjusted to its environment. Each sonde was then plotted and examined manually. This revealed a handful of sondes with relative humidity below 10% at the lowest level before splashdown, but with more typical values near 80% immediately above. Those few erroneous near-surface humidity data were removed as well. The original data from Editsonde generally contained 0.5-s time resolution (about 10 m). These data were interpolated to 100-m levels in the vertical following Molinari and Vollaro (2010). Linear interpolation of temperature and dewpoint was performed across gaps of up to 400 m. No CAPE or buoyancy was calculated from soundings with larger gaps. After this processing, 2458 sondes remained for analysis.

Soundings processed using Editsonde software have been compared with those processed with the Atmospheric Sounding Processing Environment (ASPEN; <http://www.atd.ucar.edu/sssf/facilities/software/asp/asp.html>) by Schneider and Barnes (2005). They found only small differences between the two. Neither processing program addresses the occasional problem of saturated, near dry-adiabatic layers below cloud base (Barnes 2008), which existed in 3.3% of the sondes in this study. These were corrected following the method of Bogner et al. (2000) [see Molinari and Vollaro (2010) for an example of this correction].

The sounding temperatures above the sonde release point were defined by bilinearly interpolating the temperature lapse rate from the nearest 6-h time of the interim European Centre for Medium-Range Weather Forecasts (ECMWF) Re-Analysis (ERA-Interim) gridded analyses (Simmons et al. 2007) to the sounding location for levels above the first sonde observation level, following Molinari and Vollaro (2010). Relative humidity above the sonde release point, as well as missing values of relative humidity in the upper troposphere, were taken as 100%; this assumption had negligible impact on CAPE calculations owing to the small saturation vapor pressure at those high levels.

CAPE often contains a major contribution from the upper troposphere. For instance, Bogner et al. (2000) used GPS sondes released from about 450 hPa, and appended mean hurricane soundings above that level. They found that two-thirds of (pseudoadiabatic) CAPE was found above the mean sonde release level. The G-IV sondes in this study have a mean release elevation of 13.06 km (near 180 hPa) with a standard deviation of 0.59 km. This insures that most of the troposphere is represented by directly measured sounding values rather than by the layer added from ERA-Interim.

Ambient vertical wind shear was taken from the Statistical Hurricane Intensity Prediction Scheme (SHIPS) database (DeMaria et al. 2005). It represents an average over 500 km that removes the representation of the cyclone. The percentages of sondes in this study that were released in the presence of weak (less than 5 m s^{-1}), moderate ($5\text{--}10 \text{ m s}^{-1}$), and strong ($>10 \text{ m s}^{-1}$) ambient shear were 39%, 48%, and 13%, respectively. These percentages were slightly lower for weak and strong shear, and larger for moderate shear, than those in Hanley et al. (2001) and Abarca et al. (2011).

The radius from the storm center and the azimuthal position with respect to the ambient shear were determined for each sonde following Molinari and Vollaro (2010). Figure 1 shows the locations of these sondes, with downshear to the right. The distribution of sondes is relatively uniform in radius and azimuth, with 53% of

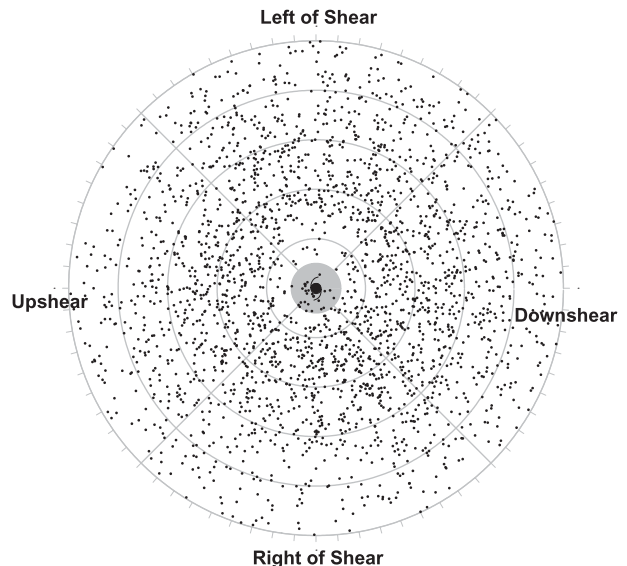


FIG. 1. Location of dropsondes with respect to the storm centers, and rotated with respect to the ambient vertical shear vector. Gray lines define the quadrants with respect to shear, with downshear to the right. Range rings are at 200-km increments. The shaded region lies inside the 100-km radius. The hurricane symbol represents the storm center.

sondes downshear. The results will be presented in 100-km radial bins.

Figure 2 shows the number of sondes in each bin. Only 27 sondes were released inside the 100-km radius. As a result, the analysis in this study will be restricted to outside this radius. That eliminates the convective maximum in the eyewall region in hurricane-strength storms (e.g., Molinari et al. 1999; Abarca et al. 2011). A convective minimum occurs from 80- to 100-km radii on average in hurricanes, and over a larger region (80–160 km) in prehurricane disturbances (Abarca et al. 2011). Beyond that radius flash density increased outward to radius $r = 250\text{--}300 \text{ km}$ in the convectively active outer rainbands. Molinari et al. (1994, 1999) found that the flash density maximum was almost always within 300 km of the center. No studies have examined flash rates beyond $r = 300 \text{ km}$, but Cecil et al. (2002) showed that outer band flash density is more than 4 times that in the average subtropical environment (column 2 of their Table 4). Frank (1977) examined hourly precipitation data from small Pacific islands experiencing typhoon passage. He used 2° latitude (222 km) increments as a measure of radius. He found that rainfall exceeded 7.6 mm h^{-1} 16% of the time within 222 km. This was 2.7 times more frequent than for 222–444 km, 6 times more than 444–666 km, and 10 times more frequent than beyond 666 km. To the extent that these represent convective rain events, this indicates a rapid decrease in the frequency of deep

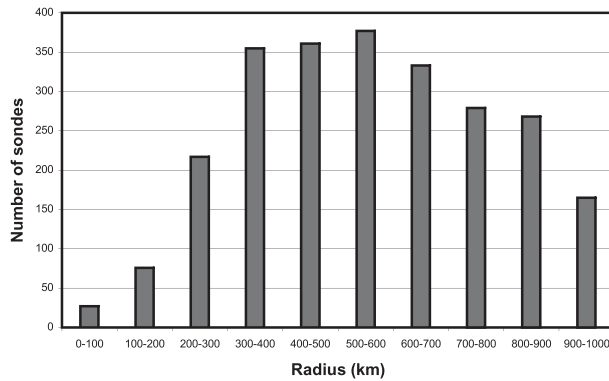


FIG. 2. Number of sondes in each radial bin.

convection with radius to a minimum beyond $r = 666$ km. All of these regions are well represented by the sondes in this study. CAPE and buoyancy will be calculated from the 100–1000-km radii.

Even in a tropical cyclone, the percentage coverage of active deep convection is on the order of 10% or less (e.g., Malkus et al. 1961; Table 3 of Jorgensen et al. 1985; Black et al. 1996; Rogers et al. 2012), especially outside the eyewall region. The large number of sondes in this study represents a benefit in that both the mean and the 90th percentile of CAPE and CIN can be examined. These values might be more representative of the actual regions supportive of active deep clouds in storms.

b. Calculation of CAPE and buoyancy

Buoyancy profiles for lifted parcels are calculated as described in the appendix of Romps and Kuang (2010). Since those equations include a fully prognostic momentum equation, we have replaced the momentum equation with $dw/dt = 0$ and initialized parcels with a vertical velocity of 1 m s^{-1} to ensure traversal of the entire troposphere; this has no effect on the parcel's buoyancy aside from altering an already negligible amount of frictional dissipation. There are three free parameters in the model: the fraction of condensed water that falls out of the parcel γ , the fractional entrainment rate ε , and the temperature at which all condensates are assumed to be frozen. In the “no fallout” case ($\gamma = 0$), all of the condensates are retained in the parcel. In the “total fallout” case ($\gamma = 1$), all condensates are removed from the parcel immediately upon formation. For $\varepsilon = 0$, the no fallout and total fallout cases correspond to reversible adiabatic and pseudoadiabatic ascent, respectively. In the “with fusion” cases, all retained and newly formed condensates transition linearly from liquid to ice between 273.15 and 240 K. In the “without fusion” cases, the heat capacity of ice is set to that of liquid water and

the latent heat of fusion is set to zero. All parcels are lifted from $z = 100$ m, which has been argued to be the appropriate initial height for CAPE calculations (Romps and Kuang 2011). When the properties of the initial parcel were instead defined by mixing air between 100 and 500 m, the magnitude of CAPE decreased, but the radial shape of the CAPE distributions remained the same.

CAPE is defined as the vertical integral of all positive buoyancy values between 100 m and the level of neutral buoyancy (LNB). The calculation of CIN is more complex. If no CAPE exists, CIN has little meaning. But comparing CIN among various parcel calculations is then not possible, because CAPE might exist, for instance, when fusion is included but not otherwise. The CIN calculations would then represent different samples of cases depending upon the physics of the parcel calculation. CIN is instead calculated up to a fixed level of $z = 1.5$ km, regardless of whether CAPE is nonzero. CIN is defined as the minimum kinetic energy required to reach that level starting at $z = 100$ m. Under the typical circumstances of negative area ending below 1.5 km and positive area above in the lower troposphere, this definition is equivalent to summing the negative areas up to 1.5 km. But when a parcel experiences, for instance, adjacent layers of negative, positive, and negative regions below 1.5 km as it rises, this calculation gives smaller CIN than simply summing the negative area. This gives a more accurate estimate of the minimum kinetic energy needed for the parcel to reach a given level.

A bootstrap method (e.g., Wilks 1995) was used to determine the significance of upshear–downshear differences in CAPE and CIN. Assume for a given radial bin that $n + m$ sondes were present, n downshear and m upshear. A random group of n and a random group of m were chosen (with replacement) from the $n + m$ sondes, and the difference in the mean values of the two groups was recorded. That step was repeated 10 000 times. The upshear–downshear difference at each radius was significant at the 5% level if it fell outside of the 2.5th–97.5th percentiles of the distribution of the 10 000 differences.

c. Slantwise versus upright CAPE

In tropical cyclones, the surfaces of equivalent potential temperature θ_e and absolute angular momentum slope outward, and a symmetrically neutral parcel moves outward with height (e.g., Emanuel 1986; Marks et al. 1992). Upright buoyancy is less than slantwise buoyancy owing to upper-tropospheric warming in the storm core. Slantwise convection cannot be calculated in this work because it requires a field of soundings in each

storm rather than soundings in multiple storms. A simple calculation suggests, however, that as long as some buoyancy exists, upright convection is a good approximation. An upper bound on the maximum possible radial acceleration for a parcel can be obtained by neglecting the radial pressure force altogether. This gives a maximum possible radial acceleration of $f v_\lambda + v_\lambda^2/r$, where v_λ is the tangential velocity. For $v_\lambda = 30 \text{ m s}^{-1}$ at $r = 300 \text{ km}$, assuming 20°N where the Coriolis force $f = 5 \times 10^{-5} \text{ s}^{-1}$, this maximum radial acceleration is $4.5 \times 10^{-3} \text{ m s}^{-2}$. Since this calculation completely neglects the radial pressure-gradient force, the actual radial acceleration will be much less than this. On the other hand, the vertical acceleration due to buoyancy when a parcel is 1 K warmer than an environmental temperature of 273 K is $g(T'/T) = 3.6 \times 10^{-2} \text{ m s}^{-2}$, which is one order of magnitude larger than the largest possible radial acceleration. As a result, in the presence of sufficient upright parcel buoyancy, the calculation of CAPE in a vertical column will be an accurate measure of potential kinetic energy, especially in the regions outside the storm core examined in this study.

It will be shown that a significant fraction of sondes contain upright CAPE $< 100 \text{ J kg}^{-1}$. For those, the assumption of upright convection being more applicable than slantwise might not hold. However, as noted earlier, the 90th percentile of CAPE is more relevant to regions of active deep clouds, and these CAPE values are large enough to insure the dominance of upright over slantwise convection. In addition, the results will be compared to other observations in tropical cyclones, all of which represent upright CAPE.

3. Results

a. CAPE versus radius

Figure 3 shows the variation of mean CAPE with radius in tropical cyclones for five sets of parcel paths: (i) “total fallout/undilute/no fusion” (i.e., pseudoadiabatic without fusion); (ii) “no fallout/undilute/no fusion” (i.e., reversible without fusion); (iii) “no fallout/undilute/with fusion” (i.e., reversible with fusion); (iv) “no fallout/entraining/no fusion”; and (v) “no fallout/entraining/with fusion.” The ordinate is a log axis, which is chosen to emphasize the fractional changes in CAPE with radius.

Unless otherwise specified, cases labeled “entraining” use a fractional entrainment rate of $10\% \text{ km}^{-1}$. This rate of entrainment is chosen as a compromise between higher rates ($>10\% \text{ km}^{-1}$), which give a higher sensitivity to environmental humidity, and lower rates ($<10\% \text{ km}^{-1}$), which consistently predict deep conditional instability. Numerical simulations find average

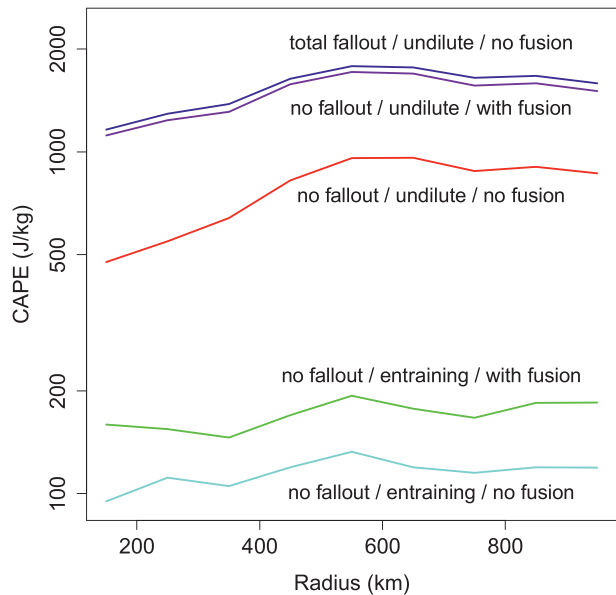


FIG. 3. Mean CAPE vs radius determined by averaging from the dropsondes shown in Fig. 1 over 100-km radial bins. Five different parcel paths are shown: blue—“total fallout/undilute/no fusion” (i.e., pseudoadiabatic without fusion), red—“no fallout/undilute/no fusion” (i.e., reversible without fusion), purple—“no fallout/undilute/with fusion” (i.e., reversible with fusion), green—“no fallout/entraining/with fusion”, and cyan—“no fallout/entraining/no fusion.”

entrainment rates on the order of $100\% \text{ km}^{-1}$ (Romps 2010), but simulations also find that the lucky updrafts that get to the tropopause experience an effective entrainment rate on the order of $5\% \text{ km}^{-1}$ (Romps and Kuang 2010). A value of $10\% \text{ km}^{-1}$ errs on the side of allowing very deep convection and will therefore give a conservative estimate of the overall effect of entrainment.

The pseudoadiabatic curve (blue line) resembles the best-fit curve of the same variable in tropical cyclones shown by Bogner et al. (2000). In agreement with that paper, the smallest CAPE ($<1200 \text{ J kg}^{-1}$) was found in the inner regions of the storm. Pseudoadiabatic CAPE increased outward to reach 1800 J kg^{-1} at $r = 500\text{--}600 \text{ km}$ and then decreased slowly to near 1600 J kg^{-1} at the outer radii.

Reversible CAPE (red line in Fig. 3) had approximately half the magnitude of pseudoadiabatic CAPE, reflecting the role of condensate loading. Adding fusion to the reversible CAPE (purple line) almost reproduced the pseudoadiabatic curve. This result supports the conclusions of Williams and Renno (1993) and Emanuel (1994) that the effects of fusion and water loading seem to offset one another when all condensate remains with the parcel. The shape of the radial distribution was

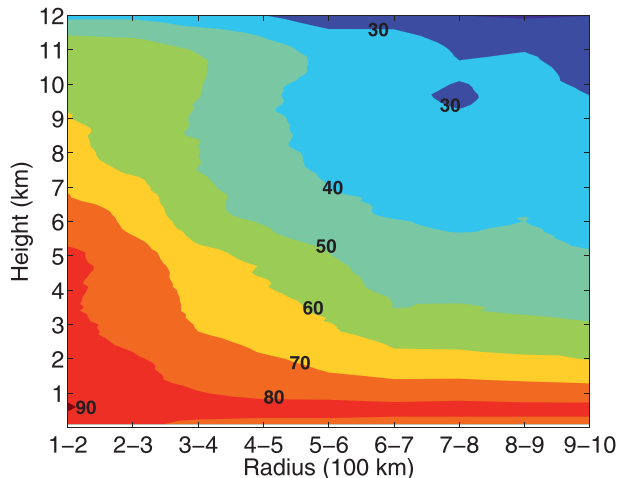


FIG. 4. Mean relative humidity vs radius in tropical cyclones using the dropsondes in Fig. 1, shown as a contour of points representing the average of sondes within 100-km radial bins and 100-m vertical layers. This figure is taken from the work of Nguyen et al. (2010).

similar in each of the three curves discussed above, with maximum CAPE near the 600-km radius.

The lower curves of Fig. 3 differed dramatically as a result of the inclusion of a fractional rate of entrainment of $10\% \text{ km}^{-1}$. Adding entrainment without fusion heating (cyan line) reduced mean CAPE by a factor of 5 at inner radii and a factor of 10 at outer radii. Entraining CAPE at outer radii had a similar magnitude to that in the core, producing a flattening of the radial profile. Within a range of entrainment values from 5% to $20\% \text{ km}^{-1}$, doubling the entrainment rate reduced mean CAPE by a factor of 2. The flattening of the radial profile of CAPE occurred for all entrainment rates within that range.

Adding fusion heating to the calculation (no fallout/entraining/with fusion; green line in Fig. 3) approximately doubled the magnitude of entraining CAPE. Nevertheless, fusion had much less impact for entraining CAPE than it did for reversible CAPE (cf. the difference between the red and purple lines in Fig. 3 vs the cyan and green lines) because entraining parcels had less water per unit mass available to freeze.

Note, from Fig. 3, that the radial distributions of CAPE for undilute ascent share a peculiar pattern: the mean CAPE rises a dramatic 50%–100% from a radius of 100–200 km to a radius of 500–700 km. All else being equal, this would tend to generate convection that is more vigorous and more frequently deep at 500–700 km than at smaller radii. This belies the 6–10-times-less-frequent heavy rain events at these radii compared with inner radii, as found by Frank (1977). When entrainment is added to the parcel ascent, the radial distributions of

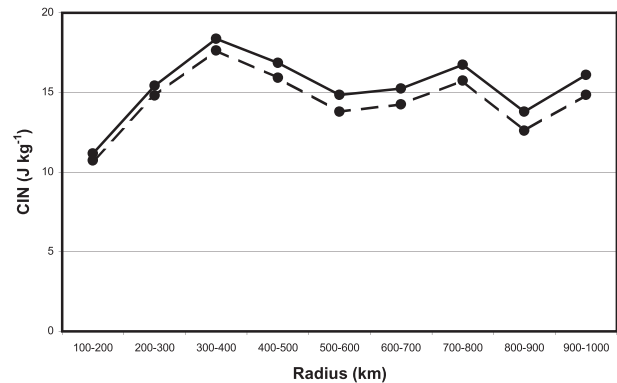


FIG. 5. Mean CIN for a parcel raised from $z = 100$ m to 1.5 km vs radius for “no fallout/undilute” (dashed) and “no fallout/entraining” (solid). See text for CIN definition.

mean CAPE vary by less than 30%–40% without any strong trend.

The reasons for the altered radial distribution of CAPE when entrainment effects were included becomes apparent in Fig. 4 [taken from Nguyen et al. (2010)]. This shows the radial–vertical variation of mean relative humidity in tropical cyclones from the same G-IV dataset used for the CAPE calculations. Figure 4 resembles an analogous composite using rawinsondes by Frank (1977). In the midtroposphere ($z = 5$ km), relative humidity decreased outward from above 80% at 100–200-km radii to below 50% at 900–1000-km radii. This latter value is representative of the tropical mean sounding values of Jordan (1958) and Dunion and Marron (2008). Entrainment of the increasingly dry air with radius reduced CAPE far more at outer radii than in the storm core. This flattened the radial distribution of CAPE.

The values of CAPE with entrainment were dramatically smaller than without. However, using the formula relating CAPE to maximum vertical velocity,

$$w_{\max} = (2\text{CAPE})^{1/2}, \quad (1)$$

yields $w_{\max} = 20 \text{ m s}^{-1}$ for a CAPE value of 200 J kg^{-1} . Although this estimate must be reduced owing to the impact of the vertical perturbation pressure gradient force, even half this value represents a large vertical velocity value in tropical cyclones (e.g., Jorgensen et al. 1985; Houze et al. 2009; Heymsfield et al. 2010; Rogers et al. 2012). The assumption of a constant entrainment rate in this study represents a considerable simplification of an extremely complex process [see, e.g., Houze (1993)]. Nevertheless, Fig. 3 shows that the influence of entrainment is too large to ignore in CAPE calculations.

Figure 5 shows the radial distribution of CIN with and without entrainment. Mean CIN was about 11 J kg^{-1} at

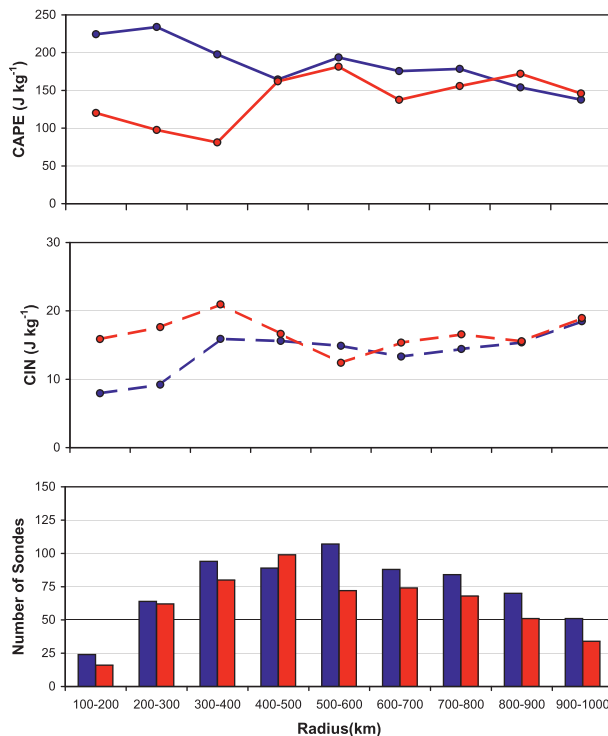


FIG. 6. (top) CAPE and (middle) CIN using “no fallout/entraining/with fusion” vs radius for upshear (red) and downshear (blue) quadrants. (bottom) Number of sondes in each quadrant.

the innermost radius in this study, and nearly constant at values of $13\text{--}18\text{ J kg}^{-1}$ at all other radii. To overcome 15 J kg^{-1} would require a 5.5 m s^{-1} updraft [Eq. (1)]. In practice, this is more likely to be achieved at smaller radii where turbulent kinetic energy is larger. Loruso et al. (2010) and Rogers et al. (2012) found turbulent kinetic energy of about $15\text{ m}^2\text{ s}^{-2}$ in the eyewall, with a secondary maximum near $8\text{ m}^2\text{ s}^{-2}$ in rainbands outside the storm core.

The inclusion of entrainment had little impact on CIN and its radial profile. This insensitivity of CIN to entrainment is a consequence of two facts. First, the inhibition layer sits above a dry boundary layer that is fairly well mixed, so entrainment has a negligible effect below the inhibition layer. Second, the inhibition layer and the region over which it is sampled (1.5 km) are both relatively narrow compared to the inverse of the fractional entrainment rate that is used here.

b. Upshear–downshear differences in CAPE

The results in this section consider only one form of CAPE: no fallout/entraining/with fusion. Figure 6 shows mean CAPE and mean CIN versus radius for upshear and downshear quadrants only (see Fig. 1 for definition of the quadrants). Outside the 400-km radius, upshear

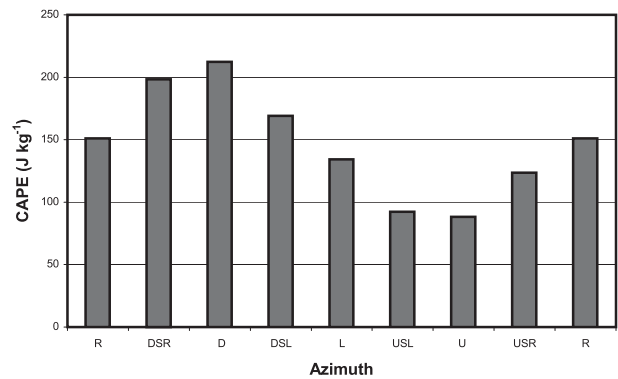


FIG. 7. Azimuthal variation of mean CAPE between 200- and 400-km radii for “no fallout/entraining/with fusion.” Quadrants rotate counterclockwise from right of shear to downshear to left of shear to upshear, with intermediate overlapping quadrants in between.

and downshear CAPE did not have significant differences at the 95% level using the bootstrap technique (see section 2 for details). Within that radius, however, downshear values were significantly larger than upshear values by about a factor of 2 at radii of 200–300 and 300–400 km. Downshear CAPE was also much larger at 100–200-km radii but failed the significance test because the sonde number was too low. The upshear–downshear differences in CIN were not significant outside the 300-km radius, but downshear values were significantly smaller than upshear values by a factor of 2 from 200 to 300 km and fell just short of significance for the 100–200-km radii. Figure 6 indicates that mean values of both CAPE and CIN favor more convection downshear than upshear.

Figure 7 shows the azimuthal variation of the same measure of CAPE as in Fig. 6, averaged over 200–400-km radii where upshear and downshear values differed significantly. The results are shown by quadrant, shifting counterclockwise from right of shear to downshear to left of shear to upshear, with intermediate overlapping quadrants in between. Figure 7 shows larger CAPE downshear and right of the shear vector than upshear and left of the shear vector. Downshear contained the maximum CAPE and upshear the minimum. The CAPE distribution in Fig. 7 matches closely the azimuthal lightning distribution from 100 to 300 km found by Corbosiero and Molinari (2003; see the top right panel of their Fig. 7), with larger mean CAPE aligning with a greater lightning frequency.

One striking aspect of Fig. 6 is that the largest CAPE existed downshear at inner radii where convection is most frequent, and CAPE decreased outward as the subtropical environmental values were approached. The smallest CAPE occurred upshear at inner radii. As a result, this form of CAPE best reflected where persistent convection

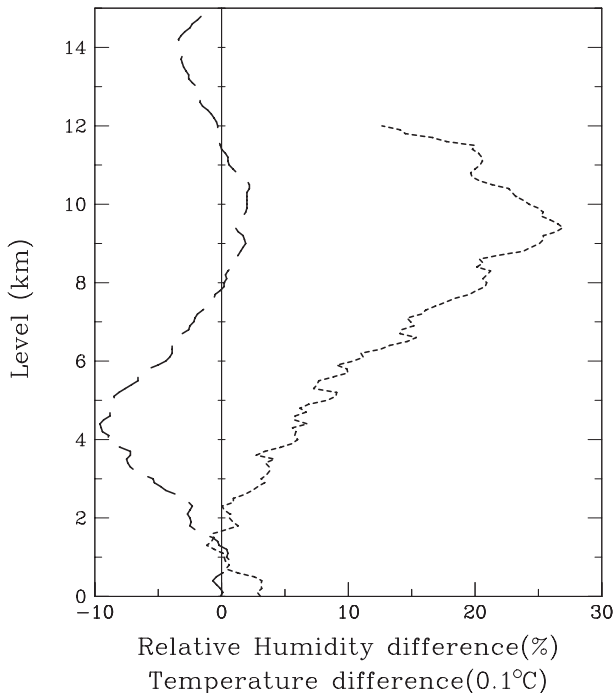


FIG. 8. Vertical profiles of downshear-minus-upshear differences in temperature (long dashed) and relative humidity (short dashed), averaged over radii from 200 to 400 km.

arises in tropical cyclones. All combinations of entraining CAPE (with or without condensate loading and/or fusion heating) exhibited this characteristic (not shown), whereas all undilute CAPE calculations showed an increase of CAPE with radius to a maximum near 600 km.

Figure 8 addresses the reasons for the larger CAPE downshear than upshear. Shown are the differences in mean temperature and relative humidity between the downshear and upshear quadrants. Downshear contained lower temperatures than upshear from 1- to 8-km altitude. This temperature difference peaks at 1 K at a height of 4.5 km. Other factors being equal, this would create more CAPE downshear. Although near-surface temperatures in Fig. 8 were about the same upshear and downshear, relative humidity was larger downshear by 3%. This higher relative humidity in the downshear boundary layer gives parcels a higher θ_e by about 1.5 K (assuming a temperature of 300 K), which also contributed to a larger CAPE downshear. Finally, for entraining CAPE, the moister air in the downshear free troposphere reduced the impact of entrainment versus upshear.

Using the same dropsonde data, the mean wind speed within 20 m of the surface from $r = 200$ to 400 km was larger downshear than upshear by 1.9 m s^{-1} (about 16%).

Given the same sea surface temperature and the same surface-air relative humidity, the higher wind speed downshear would produce larger surface fluxes there. Given the same advection tendencies and boundary layer ventilation, this would tend to make the boundary layer more humid downshear than upshear. This fits the observation of a larger specific humidity downshear versus upshear, as shown in Fig. 8.

Figure 9 shows scatterplots of CAPE and CIN for $r = 200$ –400 km for upshear and downshear quadrants. Red circles indicate values in the lowest 10% of CIN, yellow the largest 10% of CAPE, and blue circles where both conditions are met. In both regions CIN and CAPE are negatively correlated. The majority of large CIN values ($>40 \text{ J kg}^{-1}$) in both regions coexist with zero or near-zero CAPE. Similarly, the largest values of CAPE most often occur with zero or near-zero CIN. This inverse relationship between CAPE and CIN was also shown in predepression disturbances by Smith and Montgomery (2012).

Figure 9 shows a substantial difference in the CAPE distributions between upshear and downshear. The downshear CAPE distribution displayed a long tail of larger values above 500 J kg^{-1} , whereas no values exceeded 500 J kg^{-1} upshear. As noted earlier, tropical cyclones typically experience deep convection over a fractional area on the order of 10%. The upper 10% of CAPE values averaged 725 J kg^{-1} downshear and 341 J kg^{-1} upshear. CAPE calculated from the 90th percentile of buoyancy at each level varied similarly at 620 and 327 J kg^{-1} , respectively. Stated simply, the most unstable soundings downshear were twice as unstable as the most unstable soundings upshear. The CIN distribution differed from CAPE in that the lowest 10% of CIN values (red circles) were zero or nearly zero both downshear and upshear. As a result, the observed difference in lightning frequency between upshear and downshear quadrants does not seem to relate to variations in the distribution of CIN.

c. Vertical profiles of buoyancy

As we have seen in Fig. 3, different modes of parcel ascent predict wildly different magnitudes of CAPE. Which definition of CAPE is most representative of the conditions experienced by moist convection in tropical cyclones? To address this question, we will evaluate different modes of parcel ascent against two observations: 1) tropical cyclones contain deep convection over a fractional area on the order of 10%; and 2) lightning strikes are 6 times more frequent downshear than upshear between 200 and 400 km of the storm center (Corbosiero and Molinari 2003; Abarca et al. 2011).

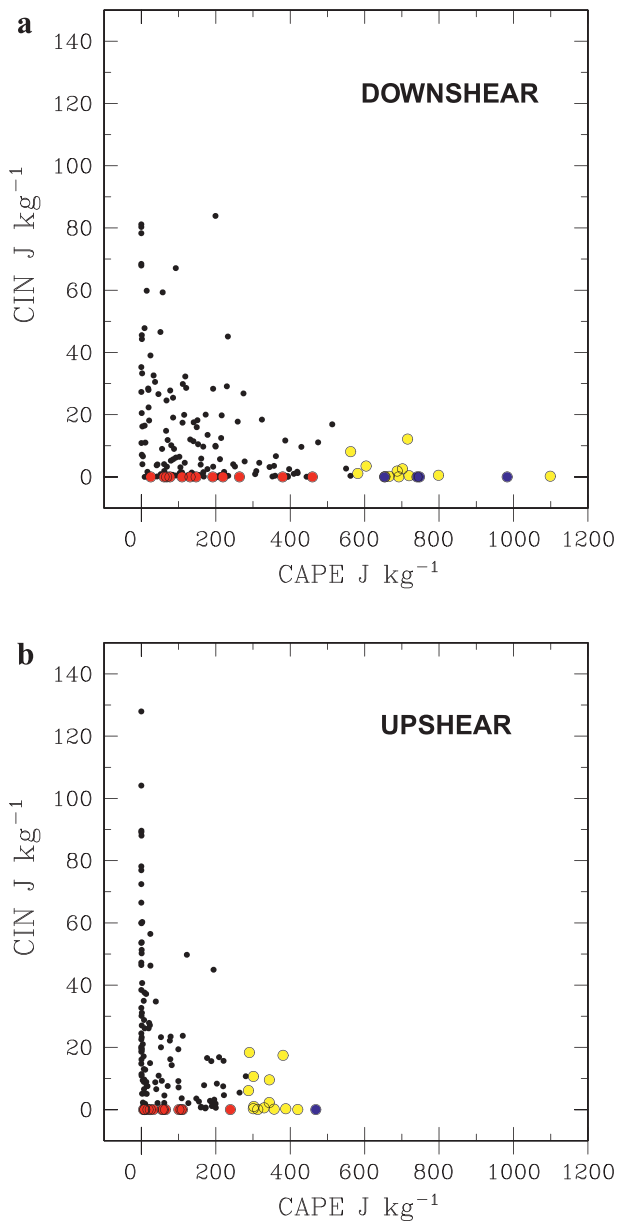


FIG. 9. Scatterplot of CIN and CAPE between 200- and 400-km radii for the (top) downshear and (bottom) upshear quadrants. Red circles indicate the lowest 10% of CIN values for each region, yellow circles indicate the top 10% of CAPE values, and blue circles represent both conditions being satisfied.

Here, we focus specifically on the region between 200 and 400 km of the storm center, where upshear-downshear CAPE differences were greatest (Fig. 6). The first observation suggests that at least 10% of the soundings should exhibit the potential for deep convection. Therefore, if we look at the soundings in the top 10% of conditional instability, the method we use for calculating the buoyancy of lifted parcels (and, therefore, CAPE) should find positive buoyancy above 11 km

(i.e., into the top third of the troposphere). Next, we expect the differences between upshear and downshear lightning frequencies to be explained, at least in part, by differences in upshear and downshear CAPE. All else being equal, larger CAPE promotes more deep convection. Also, larger CAPE produces more vigorous convection, which promotes more lightning (Williams et al. 1992; Rutledge et al. 1992). Therefore, this second observation suggests that the CAPE of the top 10% of soundings should be much larger downshear than upshear. To be quantitative, we require the ratio of the downshear and upshear CAPE at the 90th percentile to be at least 2. Baker et al. (1995; 1999) found that lightning flash frequency was proportional to w^6 , and thus $(\text{CAPE})^3$. The factor of 2 supports a factor of 8 difference in lightning frequency, close to that observed.

At each height, the collection of soundings in a particular quadrant gives a distribution of buoyancies for lifted parcels at that height. We form a composite buoyancy profile by picking the 90th percentile of this distribution at each height. This composite profile closely resembles the buoyancy profile of the lifted parcel with the 90th percentile of overall CAPE, but the compositing eliminates much of the noise and idiosyncracies associated with any one profile.

Between 200 and 400 km from the storm center, there are 158 soundings in the downshear quadrant and 142 soundings in the upshear quadrant. Figure 10 shows the composited 90th-percentile buoyancy profiles calculated from these data. These buoyancy profiles are shown for 16 different modes of parcel ascent corresponding to all possible combinations of total fallout (first and second columns) and no fallout (third and fourth columns), no fusion (first and third columns) and with fusion (second and fourth columns), and fractional entrainment rates of (top to bottom) 0%, 5%, 10%, and 20% km⁻¹. Solid lines correspond to the 90th-percentile buoyancy downshear and dashed lines correspond to the 90th-percentile upshear. We can evaluate these plots against the two criteria previously described.

Since deep convective updrafts occupy on the order of 10% of a hurricane's area, at least 10% of the area must be conditionally unstable to deep convection. Therefore, we can rule out any mode of ascent that does not give any positive buoyancy above 11 km. For example, this definitively rules out using entrainment rates equal to 20% km⁻¹ or higher: all of the 90th-percentile profiles calculated with an entrainment rate of 20% km⁻¹ are negatively buoyant above 8 km. This result is consistent with the much larger values of average entrainment obtained from numerical studies (Romps and Kuang 2010; Romps 2010) because cloudy parcels experience a wide range of effective entrainment rates. As noted

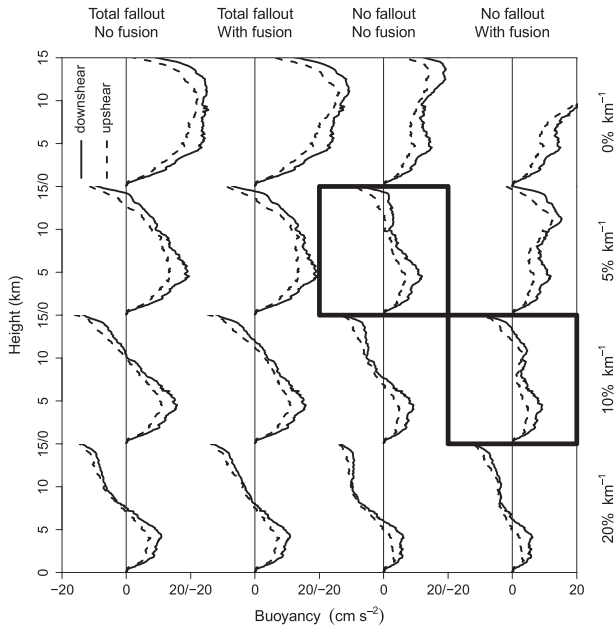


FIG. 10. Profiles of 90th-percentile buoyancy between 200- and 400-km radii for the downshear (solid) and upshear (dashed) quadrants. Buoyancy profiles are shown as calculated in 16 different ways corresponding to the 16 different combinations of total fallout (first and second columns) vs no fallout (third and fourth columns), no fusion (first and third columns) vs with fusion (second and fourth columns), and entrainment rates of (top to bottom) 0%, 5%, 10%, and 20% km^{-1} . Thick-outlined boxes highlight the two cases in which deep convection is buoyant above 11 km and CAPE is twice as large downshear as upshear.

earlier, Romps and Kuang (2010) found that the parcels reaching the tropopause experienced an effective entrainment rate as small as 5% km^{-1} .

The second criterion requires that the integrated buoyancy (CAPE) of the downshear profile be twice that of the upshear profile. By visual inspection, this rules out all of the undiluted (i.e., 0% km^{-1}) calculations as well as all of the “total fallout” calculations. Therefore, to satisfy both criteria, we conclude that we must retain condensates (i.e., use “no fallout”) and we must use a nonzero entrainment rate less than 20% km^{-1} . In fact, only two calculations simultaneously satisfy both criteria: no fallout/5% km^{-1} /no fusion and no fallout/10% km^{-1} /with fusion, which are highlighted by thick-outlined boxes in Fig. 10. This suggests that a one-parameter family of solutions may be equally suitable, with entrainment ranging from 5% to 10% km^{-1} as the amount of fusion heating is varied from none to all. Therefore, we conclude that vigorous deep convection in tropical cyclones is most accurately represented by updrafts ascending with the following characteristics: total condensate retention, an entrainment rate between 5% and 10% km^{-1} , and an amount of fusion heating

somewhere between zero (appropriate at 5% km^{-1}) and its maximal value (appropriate at 10% km^{-1}).

4. Discussion

Following the procedures of Romps and Kuang (2010), CAPE and CIN were calculated with and without the influence of condensate loading, entrainment of environmental air, and heating associated with the freezing of condensate. The data for these calculations came from more than 2000 dropsondes released from the upper troposphere in tropical cyclones of all intensities.

Reversible CAPE without fusion had only one-half the magnitude of pseudoadiabatic CAPE without fusion. Consistent with Williams and Renno (1993) and Emanuel (1994), reversible CAPE with fusion closely resembled pseudoadiabatic CAPE without fusion. Both pseudoadiabatic and reversible CAPE showed maxima at the 600–700-km radius. Tropical cyclones contain one order of magnitude fewer heavy rain events at those radii than in the inner 222 km (Frank 1977). The addition of entrainment to the CAPE calculation had the dramatic impact of removing this outer radius maximum. All forms of entraining CAPE produced an outward decrease of downshear CAPE from an inner core maximum. Entraining CAPE was thus more consistent with the observed radial distribution of convection in tropical cyclones.

Previous studies have shown that lightning in tropical cyclones is 6 times more frequent downshear than upshear within 300 km of the center. Mean CAPE calculated with entrainment and fusion showed substantially larger values downshear, in agreement with the lightning statistics. The azimuthal distribution of entraining CAPE by octant within 200–400 km of the center (Fig. 7) matched well the distribution of lightning from 100- to 300-km radii found by Corbosiero and Molinari (2003), with larger CAPE associated with greater flash density per unit time. The larger entraining CAPE downshear arose from (see Fig. 8) (i) higher surface specific humidity, (ii) lower midtropospheric temperature, and (iii) larger free-tropospheric relative humidity, which reduced the impact of entrainment on parcel buoyancy.

Because convection consumes CAPE, enduring downshear convection is possible only if forcing restores CAPE. Vertical wind shear creates enhanced upward motion downshear in cyclonic disturbances (Raymond and Jiang 1990; Trier et al. 2000), and evidence for such downshear upward motion has clearly been shown in tropical cyclones (Black et al. 2002; Frank and Ritchie 1999). Such upward motion would generate the lower temperatures and higher humidity (Fig. 8) that help to create downshear

CAPE. In addition, the larger surface moisture content downshear (Fig. 8) is consistent with larger forcing via ocean fluxes, which is supported by the larger wind speeds downshear (section 3b). By this reasoning, persistent downshear convection is possible only because forcing by upward motion and enhanced surface fluxes maintains CAPE against its consumption by the convection. Once entrainment is included in the parcel evolution in tropical cyclones, this expected positive correlation between CAPE and vigorous deep convection is realized.

Tropical cyclones are observed to have active convection over less than 10% of their area, especially at the radii outside 100 km considered here. The large number of sondes in this study allowed for the examination of the 90th percentile of CAPE, CIN, and buoyancy, which is relevant to the 10% areal coverage of convection. Only by including condensate loading and a fractional entrainment rate in the range of 5%–10% km⁻¹ did the profiles of 90th-percentile buoyancy reflect the observed distribution of convection and lightning. With that combination of processes, the 90th-percentile profiles at a radius of 200–400 km produced levels of neutral buoyancy above 11 km with twice as much CAPE downshear as upshear, implying 8 times the lightning frequency (Baker et al. 1999). In contrast, the lowest 10% of CIN values were near zero both upshear and downshear, indicating that CIN variation played a lesser role.

Smith and Montgomery (2012) found no clear relationship between the magnitude of pseudoadiabatic CAPE and the development of tropical cyclones from predepression disturbances. They did note, however, a much drier midtroposphere in nondeveloping disturbances. It seems likely based on the results of this paper that those disturbances would show much smaller CAPE once the role of entrainment is included. Entraining CAPE might provide a useful tool for understanding the potential for deep convection and its role in tropical cyclone formation and intensification.

Acknowledgments. We are indebted to Dr. Sim Aberson of the Hurricane Research Division of NOAA for his processing and storage of G-IV dropsonde data. ERA-Interim gridded analyses were obtained from the National Center for Atmospheric Research, which is supported by the National Science Foundation (NSF). DMR's work was supported by Laboratory Directed Research and Development (LDRD) funding from Lawrence Berkeley National Laboratory, provided by the Director, Office of Science, of the U.S. Department of Energy under Contract DE-AC02-05CH11231. JM's work was supported by NSF Grant ATM0855718.

REFERENCES

- Abarca, S. F., K. L. Corbosiero, and D. Vollaro, 2011: The World Wide Lightning Location Network and convective activity in tropical cyclones. *Mon. Wea. Rev.*, **139**, 175–191.
- Baker, M. B., H. J. Christian, and J. Latham, 1995: A computational study of the relationships linking lightning frequency and other thundercloud parameters. *Quart. J. Roy. Meteor. Soc.*, **121**, 1525–1548.
- , A. M. Blyth, H. J. Christian, J. Latham, K. L. Miller, and A. M. Gadian, 1999: Relationships between lightning activity and various thundercloud parameters: Satellite and modeling studies. *Atmos. Res.*, **51**, 221–236.
- Barnes, G. M., 2008: Atypical thermodynamic profiles in hurricanes. *Mon. Wea. Rev.*, **136**, 631–643.
- Black, M. L., R. W. Burpee, and F. D. Marks Jr., 1996: Vertical motion characteristics of tropical cyclones determined with airborne Doppler radial velocities. *J. Atmos. Sci.*, **53**, 1887–1909.
- , J. F. Gamache, F. D. Marks Jr., C. E. Samsury, and H. E. Willoughby, 2002: Eastern Pacific Hurricanes Jimena of 1991 and Olivia of 1994: The effect of vertical shear on structure and intensity. *Mon. Wea. Rev.*, **135**, 2291–2312.
- Bogner, P. B., G. M. Barnes, and J. L. Franklin, 2000: Conditional instability and shear for six hurricanes over the Atlantic Ocean. *Wea. Forecasting*, **15**, 192–207.
- Cecil, D. J., E. J. Zipser, and S. W. Nesbitt, 2002: Reflectivity, ice scattering, and lightning characteristics of hurricane eyewalls and rainbands. Part I: Quantitative description. *Mon. Wea. Rev.*, **130**, 769–784.
- Corbosiero, K. L., and J. Molinari, 2002: The effects of vertical wind shear on the distribution of convection in tropical cyclones. *Mon. Wea. Rev.*, **130**, 2110–2123.
- , and —, 2003: The relationship between storm motion, vertical wind shear, and convective asymmetries in tropical cyclones. *J. Atmos. Sci.*, **60**, 366–376.
- DeMaria, M., 2009: A simplified dynamical system for tropical cyclone intensity prediction. *Mon. Wea. Rev.*, **137**, 68–82.
- , M. Mainelli, L. K. Shay, J. A. Knaff, and J. Kaplan, 2005: Further improvements to the Statistical Hurricane Intensity Prediction Scheme (SHIPS). *Wea. Forecasting*, **20**, 531–543.
- Dunion, J. P., and C. S. Marron, 2008: A reexamination of the Jordan mean tropical sounding based on awareness of the Saharan air layer: Results from 2002. *J. Climate*, **21**, 5242–5253.
- Emanuel, K. A., 1986: An air–sea interaction theory for tropical cyclones. Part I: Steady-state maintenance. *J. Atmos. Sci.*, **43**, 585–604.
- , 1994: *Atmospheric Convection*. Oxford University Press, 580 pp.
- Fierro, A. O., E. J. Zipser, M. A. LeMone, J. M. Straka, and J. Simpson, 2012: Tropical oceanic hot towers: Need they be undilute to transport energy from the boundary layer to the upper troposphere effectively? An answer based on trajectory analysis of a simulation of a TOGA COARE convective system. *J. Atmos. Sci.*, **69**, 195–213.
- Frank, W. M., 1977: The structure and energetics of the tropical cyclone. I. Storm structure. *Mon. Wea. Rev.*, **105**, 1119–1135.
- , and E. A. Ritchie, 1999: Effects of environmental flow upon tropical cyclone structure. *Mon. Wea. Rev.*, **127**, 2044–2061.
- Hanley, D., J. Molinari, and D. Keyser, 2001: A composite study of the interactions between tropical cyclones and upper-tropospheric troughs. *Mon. Wea. Rev.*, **129**, 2570–2584.

- Heymsfield, G. M., L. Tian, A. J. Heymsfield, L. Li, and S. Guimond, 2010: Characteristics of deep tropical and subtropical convection from nadir-viewing high-altitude airborne Doppler radar. *J. Atmos. Sci.*, **67**, 285–308.
- Hock, T. F., and J. L. Franklin, 1999: The NCAR GPS dropwindsonde. *Bull. Amer. Meteor. Soc.*, **80**, 407–420.
- Holloway, C. E., and J. D. Neelin, 2009: Moisture vertical structure, column water vapor, and tropical deep convection. *J. Atmos. Sci.*, **66**, 1665–1683.
- Houze, R. A., Jr., 1993: *Cloud Dynamics*. Academic Press, 573 pp.
- , W.-C. Lee, and M. M. Bell, 2009: Convective contribution to the genesis of Hurricane Ophelia (2005). *Mon. Wea. Rev.*, **137**, 2778–2800.
- Jordan, C. L., 1958: Mean soundings for the West Indies area. *J. Meteor.*, **15**, 91–97.
- Jorgensen, D. F., E. J. Zipser, and M. A. LeMone, 1985: Vertical motions in intense hurricanes. *J. Atmos. Sci.*, **42**, 839–856.
- Lorsolo, S., J. Zhang, F. D. Marks Jr., and J. Gamache, 2010: Estimation and mapping of hurricane turbulent energy using airborne Doppler measurements. *Mon. Wea. Rev.*, **138**, 3656–3670.
- Malkus, J. S., C. Ronne, and M. Chaffe, 1961: Cloud patterns in Hurricane Daisy, 1958. *Tellus*, **13**, 8–30.
- Marks, F. D., Jr., R. A. Houze Jr., and J. F. Gamache, 1992: Dual-aircraft investigation of the inner core of Hurricane Norbert. Part I: Kinematic structure. *J. Atmos. Sci.*, **49**, 919–942.
- Molinari, J., and D. Vollaro, 2010: Distribution of helicity, CAPE, and shear in tropical cyclones. *J. Atmos. Sci.*, **67**, 274–284.
- , P. K. Moore, V. P. Idone, R. W. Henderson, and A. B. Saljoughy, 1994: Cloud-to-ground lightning in Hurricane Andrew. *J. Geophys. Res.*, **99**, 16 665–16 676.
- , —, and —, 1999: Convective structure of hurricanes as revealed by lightning locations. *Mon. Wea. Rev.*, **127**, 520–534.
- Nguyen, L., D. Thomas, D. Vollaro, and J. Molinari, 2010: Thermodynamic structure of tropical cyclones from dropsondes. *Extended Abstracts, 29th Conf. on Hurricanes and Tropical Meteorology*, Tucson, AZ, Amer. Meteor. Soc., P2.42. [Available online at http://ams.confex.com/ams/29Hurricanes/techprogram/paper_167586.htm.]
- Raymond, D. J., and H. Jiang, 1990: A theory for long-lived mesoscale convective systems. *J. Atmos. Sci.*, **47**, 3067–3077.
- Rogers, R., S. Lorsolo, P. Reasor, J. Gamache, and F. Marks, 2012: Multiscale analysis of tropical cyclone kinematic structure from airborne Doppler radar composites. *Mon. Wea. Rev.*, **140**, 77–99.
- Romps, D. M., 2010: A direct measure of entrainment. *J. Atmos. Sci.*, **67**, 1908–1927.
- , and Z. Kuang, 2009: Overshooting convection in tropical cyclones. *Geophys. Res. Lett.*, **36**, L09804, doi:10.1029/2009GL037396.
- , and —, 2010: Do undiluted convective plumes exist in the upper tropical troposphere? *J. Atmos. Sci.*, **67**, 468–484.
- , and —, 2011: A transilient matrix for moist convection. *J. Atmos. Sci.*, **68**, 2009–2025.
- Rutledge, S. A., E. R. Williams, and T. D. Keenan, 1992: The Down Under Doppler and Electricity Experiment (DUNDEE): Overview and preliminary results. *Bull. Amer. Meteor. Soc.*, **73**, 3–16.
- Schneider, R., and G. M. Barnes, 2005: Low-level kinematic, thermodynamic, and reflectivity fields associated with Hurricane Bonnie (1998) at landfall. *Mon. Wea. Rev.*, **133**, 3243–3259.
- Simmons, A., S. Uppala, D. Dee, and S. Kobayashi, 2007: ERA-Interim: New ECMWF reanalysis products from 1989 onwards. *ECMWF Newsletter*, No. 110, European Center for Medium-Range Weather Forecasts, Reading, United Kingdom, 25–35.
- Smith, R. K., and M. T. Montgomery, 2012: Observations of the convective environment in developing and non-developing tropical disturbances. *Quart. J. Roy. Meteor. Soc.*, **138**, in press.
- Trier, S. B., C. A. Davis, and W. C. Skamarock, 2000: Long-lived mesoconvective vortices and their environment. Part II: Induced thermodynamic destabilization in idealized simulations. *Mon. Wea. Rev.*, **128**, 3396–3412.
- Wei, D., A. M. Blyth, and D. J. Raymond, 1998: Buoyancy of convective clouds in TOGA COARE. *J. Atmos. Sci.*, **55**, 3381–3391.
- Wilks, D. S., 1995: *Statistical Methods in the Atmospheric Sciences*. Academic Press, 467 pp.
- Williams, E. R., and N. Renno, 1993: An analysis of the conditional instability of the tropical atmosphere. *Mon. Wea. Rev.*, **121**, 21–36.
- , S. G. Geotis, N. Renno, S. A. Rutledge, E. Rasmussen, and T. Rickenbach, 1992: A radar and electrical study of tropical “hot towers.” *J. Atmos. Sci.*, **49**, 1386–1395.
- Xu, K., and K. A. Emanuel, 1989: Is the tropical atmosphere conditionally unstable? *Mon. Wea. Rev.*, **117**, 1471–1479.
- Zipser, E., 2003: Some views on “hot towers” after 50 years of tropical field programs and two years of TRMM data. *Cloud Systems, Hurricanes, and the Tropical Rainfall Measuring Mission (TRMM)*, Meteor. Monogr., No. 51, Amer. Meteor. Soc., 49–58.